

HDC: Hierarchical Distillation for Multi-level Noisy Consistency in Semi-Supervised Fetal Ultrasound Segmentation

Tran Quoc Khanh Le^{1,4*} Nguyen Lan Vi Vu^{2,4*} Ha-Hieu Pham^{3,4} Xuan-Loc Huynh⁵
Tien-Huy Nguyen^{1,4} Minh Huu Nhat Le⁶ Quan Nguyen⁷ Hien D. Nguyen^{1,4,8}

¹University of Information Technology, Ho Chi Minh city, Vietnam

²Ho Chi Minh University of Technology, Ho Chi Minh city, Vietnam

³University of Science, Ho Chi Minh city, Vietnam

⁴Vietnam National University, Ho Chi Minh city, Vietnam

⁵Boston University, MA, USA

⁶Taipei Medical University, Taipei, Taiwan

⁷Posts and Telecommunications Institute of Technology, Hanoi, Vietnam

⁸New Mexico State University, Las Cruces, NM, USA

Abstract

Transvaginal ultrasound is a critical imaging modality for evaluating cervical anatomy and detecting physiological changes. However, accurate segmentation of cervical structures remains challenging due to low contrast, shadow artifacts, and fuzzy boundaries. While convolutional neural networks (CNNs) have shown promising results in medical image segmentation, their performance is often limited by the need for large-scale annotated datasets—an impractical requirement in clinical ultrasound imaging. Semi-supervised learning (SSL) offers a compelling solution by leveraging unlabeled data, but existing teacher-student frameworks often suffer from confirmation bias and high computational costs. We propose **HDC**, a novel semi-supervised segmentation framework that integrates **Hierarchical Distillation** and **Consistency** learning within a multi-level noise mean-teacher framework. Unlike conventional approaches that rely solely on pseudo-labeling, we introduce a hierarchical distillation mechanism that guides feature-level learning via two novel objectives: (1) **Correlation Guidance Loss** to align feature representations between the teacher and main student branch, and (2) **Mutual Information Loss** to stabilize representations between the main and noisy student branches. Our framework reduces model complexity while improving generalization. Extensive experiments on two fetal ultrasound datasets, FUGC and PSFH, demonstrate that our method achieves competitive performance with significantly lower computational

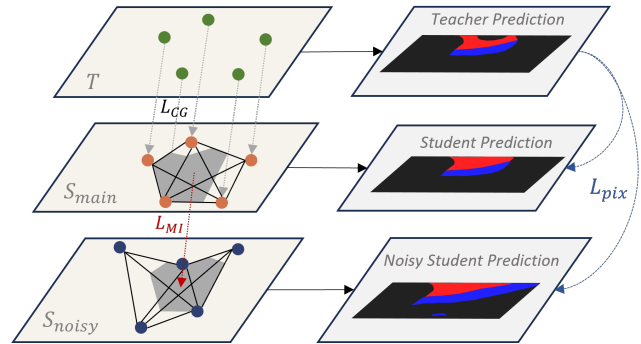


Figure 1. An intuitive overview of our Hierarchical Distillation and Consistency scheme.

overhead than existing multi-teacher models.

1. Introduction

Transvaginal ultrasound is a widely used imaging technique for assessing cervical anatomy, providing essential insights into muscle structure and function. Accurate segmentation of cervical ultrasound images is crucial for evaluating physiological changes and guiding clinical decision-making. However, the segmentation process is challenging due to common ultrasound imaging issues such as shadow artifacts, low contrast, and indistinct boundaries [1, 40].

Convolutional Neural Networks (CNNs) have demonstrated strong performance in medical image segmentation by capturing local spatial features. However, traditional supervised learning approaches that rely on CNNs require

*Equal Contribution.

large-scale annotated datasets to be generalized effectively [31]. In medical imaging, particularly in transvaginal ultrasound, obtaining pixel-wise labeled data is both time-consuming and costly, limiting the scalability of supervised CNN models [33]. Moreover, CNNs primarily focus on local dependencies, which may lead to segmentation errors such as over-segmentation or under-segmentation, particularly in complex anatomical structures.

To overcome these limitations, semi-supervised learning (SSL) has emerged as a promising approach by leveraging both labeled and unlabeled data to improve segmentation performance. Among various SSL frameworks, the Mean Teacher [39] model has gained significant attention that ensures smooth training dynamics and improves student and teacher prediction consistency. Recent advancements, such as Dual Teacher [8], introduce multiple teacher networks that periodically switch during training to enhance model robustness and mitigate confirmation bias. These techniques highlight the promise of multi-teacher SSL frameworks but add complexity or intricate update mechanisms.

Existing dual-teacher and multi-student methods [8, 51], despite their advantages, often suffer from high computational costs due to the need for training and maintaining multiple models. Some approaches address confirmation bias by incorporating strong-weak augmentation strategies or contrastive learning mechanisms. While these techniques can enhance segmentation performance, they frequently demand careful hyperparameter tuning and extensive computational resources, making them less practical for real-world medical imaging applications.

To address the challenges of semi-supervised medical image segmentation—particularly confirmation bias and computational inefficiency—this work introduces a novel framework that combines adaptive consistency training with a single-teacher architecture. Unlike conventional approaches that rely on multiple teacher-student models [8, 51], our method enhances training efficiency and generalization through structured noise injection and carefully designed objective functions. Most existing teacher-student methods focus primarily on transferring knowledge through pseudo-labeling based solely on output predictions.

In contrast, we propose a hierarchical distillation mechanism that enriches the learning signal and improves feature alignment. This is achieved through two novel loss functions: (1) **Correlation Guidance Loss**, which encourages consistency between the feature representations of the teacher and the main student branch, and (2) **Mutual Information Loss**, which aligns the representations between the main student and a noisy student branch to enhance intra-batch stability. These mechanisms are designed to bridge the feature distribution gap between teacher and student networks while stabilizing student representations in the presence of noise. HDC is evaluated on two challenging fe-

tal ultrasound datasets, FUGC and PSFH [1, 21], where it achieves **state-of-the-art** segmentation performance with significantly reduced computational overhead compared to existing methods under various evaluation metrics.

2. Related Works

Semi-Supervised Learning (SSL). The core challenge of semi-supervised learning is to maximize model accuracy while minimizing human annotation effort by effectively leveraging abundant unlabeled data in conjunction with a small set of high-quality labeled samples. Foundational works in SSL can be categorized into two dominant branches: Pseudo-labeling [2, 36] and consistency regularization [27, 29, 32]. Pseudo-labeling follows an iterative training process. The most up-to-date optimized model generates pseudo-labels from unlabeled data and combines them with labeled samples to refine prediction over time. On the other hand, consistency regularization-based methods rely on the smoothness assumption [16], stemming from the goal of training models that remain invariant to various perturbations applied to either the input data or the models themselves. FixMatch [37] integrates the strength of both strategies by employing a weak-to-strong consistency mechanism. In this research, pseudo labels are derived from weakly augmented samples and used to supervise the training of their strongly augmented counterparts. FlexMatch [49] takes into account different learning difficulties across categories and creates different thresholds for each class.

Semi-Supervised Semantic Segmentation (S4). Benefits from the advances in deep neural networks [11, 17, 44] and robust SSL algorithms, many works adopt them to build powerful semantic segmentation baselines [19, 26]. In medical image analysis, SSL also advances medicine significantly, with many noticeable works [23, 28, 29]. On top of these fundamental designs, Mean-Teacher-based methods have achieved remarkable results across benchmarks. The Mean Teacher (MT) framework [39] introduces a teacher-student architecture in which the teacher model, serving as a stable version of the student, is updated using the exponential moving average (EMA) of the student’s weights to guide the student during training. Building upon MT, PS-MT [20] proposes a stricter teacher that prevents model collapse. AD-MT [51] employs a dual-teacher framework with different perspectives in an adaptive switching manner to mitigate confirmation bias. On the other hand, co-training has also shown promising results in S4 by leveraging multi-view references to improve model perception and enhance pseudo-label reliability. Cross-pseudo supervision (CPS) [5] enforces consistency between the outputs of two networks initialized with different weights to foster diverse feature learning. CCVC [46] suggests learning richer semantic information from competing predictions by pushing the feature extractor outputs of two networks apart,

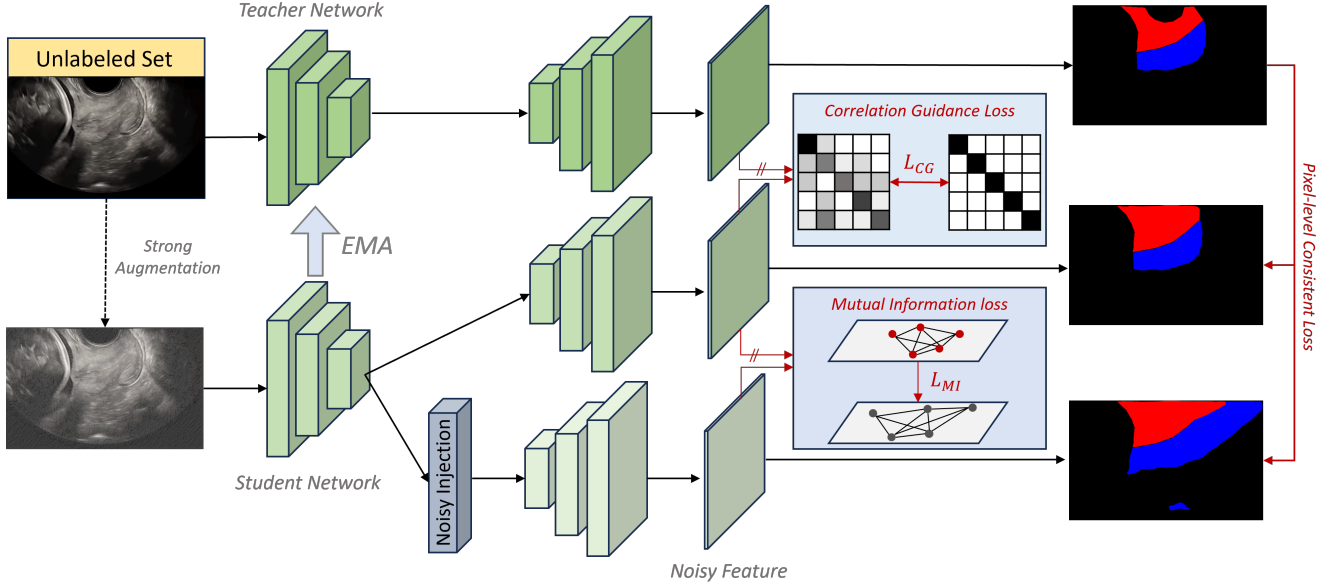


Figure 2. Our proposed semi-supervised pipeline for transvaginal ultrasound segmentation. The teacher generates pseudo-labels to guide the student, which processes both raw and noisy inputs. The dashed arrow (---) represents strong augmentation, the double slash arrow (//) denotes feature comparisons for L_{CG} and L_{MI} , black arrows indicate forward propagation, and red arrows represent pixel-level consistency loss.

thus mitigating the detrimental effects of identical coupling problems in CPS.

Knowledge Distillation (KD). Originally introduced by Hinton et al. [10], this technique enables the transfer of knowledge from a large, complex teacher model to a smaller student model, enabling efficient deployment while maintaining performance. KD plays important roles in opening new approaches for many fields such as multi-modal tasks [15, 30, 41]. Originally proposed as a method where the student mimics the teacher’s soft predictions, KD has since evolved into multiple paradigms, each capturing different aspects of knowledge transfer. KD methods are commonly categorized into logits-based [10, 14], feature-based [3, 4, 9], and relation-based approaches [12, 24]. Response-based distillation aligns the student’s predictions with the teacher’s soft outputs, often using Kullback-Leibler [42] divergence. Beyond classical approaches, recent works have explored alternative formulations grounded in self-supervision and information theory, aiming for a more structured and effective knowledge transfer. Some methods adopt orthogonal projection techniques [25] to distill knowledge more efficiently, while others focus on activation gradient alignment to better capture the loss landscape [38].

3. Method

In semi-supervised segmentation, the training set consists of a smaller labeled subset, $\mathbf{D}_l = \{(x_m^l, y_m^l)\}_{m=1}^M$, and a sig-

nificantly larger unlabeled subset, $\mathbf{D}_u = \{(x_n^u)\}_{n=1}^N$, where $N \gg M$. Each fetal ultrasound image, x_m^l or x_n^u , is represented as a tensor of size $3 \times H \times W$. Labeled images x_m^l are paired with their corresponding ground-truth segmentation masks y_m^l .

3.1. Theoretical Insights

Rényi’s Entropy [35] is a generalized measure of uncertainty that extends Shannon entropy by introducing a tunable parameter α , which adjusts the sensitivity to different probability distributions. The Rényi entropy of order α for a discrete random variable X with probability mass function $p(x)$ is defined as:

$$H_\alpha(X) = \frac{1}{1-\alpha} \log \left(\sum_{i=1}^n p_i^\alpha \right) \quad (1)$$

When $\alpha = 1$ we get the more familiar Shannon entropy $H_1(X) = \lim_{\alpha \rightarrow 1} H_\alpha(X) = -\sum_{i=1}^n p_i \log_2 p_i$.

Mutual Information (MI) [6] measures the amount of information shared between two random variables. It represents the reduction in uncertainty of one variable given knowledge of the other. Given two random variables X and Y with a joint probability mass function $p(x, y)$ and marginal distributions $p(x)$ and $p(y)$. The mutual information $I(X; Y)$ is defined as the Kullback-Leibler divergence between the joint distribution and the product of the

marginals:

$$\begin{aligned}
I(X; Y) &= \sum_{x \in \mathcal{X}} \sum_{y \in \mathcal{Y}} p(x, y) \log \frac{p(x, y)}{p(x)p(y)} \\
&= - \sum_{x, y} p(x, y) \log p(x) + \sum_{x, y} p(x, y) \log p(x|y) \\
&= H(X) - H(X|Y)
\end{aligned} \tag{2}$$

Applying the relationship between joint entropy and relative entropy, $H(X, Y) = H(Y) + H(X|Y)$, we have

$$I(X; Y) = H(X) + H(Y) - H(X, Y). \tag{3}$$

Feature-based Knowledge Distillation [7] uses latent feature representations of a high-capacity teacher model as the knowledge to supervise the training of student model. Rather than distilling knowledge from intermediate layers, we extract the final feature representations just before the fully connected layer. This preserves the structural information of the input while reducing the adverse effects of inductive biases in cross-architecture distillation.

We model the structural information through a Gram matrix $K \in \mathbb{R}^{b \times b}$, where b represents the batch size. This Gram matrix encodes the pairwise similarity among all features in a batch:

$$K_{ij} = k(\mathbf{Z}_i, \mathbf{Z}_j) = \langle \mathbf{Z}_i, \mathbf{Z}_j \rangle_{\mathcal{H}}, \tag{4}$$

where $\mathbf{Z} \in \mathbb{R}^{b \times d}$ corresponds to either teacher or student features with dimension d , and \mathcal{H} is a Hilbert space implicitly defined by the positive definite real valued kernel k , which can be selected as polynomial kernel or radial basis function kernel.

Traditional Rényi entropy is defined on probability distributions, which are often difficult to estimate in practice, especially in high-dimensional spaces where explicit density estimation is challenging. By normalizing K to have a trace of 1 and interpreting its eigenvalues $\lambda(K)$ as an implicit distribution over the feature space, we extend Rényi entropy to structured data. The matrix-based Rényi entropy is then formulated as:

$$H_\alpha(K) = \frac{1}{1-\alpha} \log_2 \left(\sum_{i=1}^n \lambda_i(K^\alpha) \right), \tag{5}$$

where $\lambda_i(K)$ are the eigenvalues of K , and α is a tunable parameter.

3.2. Overall Training Scheme

Our overall workflow is illustrated in Figure 2. The proposed HDC framework comprises a teacher network, denoted as \mathcal{T} and a single-encoder, dual-decoder student network. The student’s main decoder (\mathcal{D}_s^1) learns directly from the teacher’s representations and updates the teacher’s

weights via EMA. Meanwhile, the noisy decoder (\mathcal{D}_s^2) is trained with adversarial noise to enhance the robustness and generalization of the shared encoder \mathcal{E}_s through backward propagation.

We propose a multi-level noisy Mean Teacher framework, where noise is introduced at 3 different levels. At the lowest level, weak augmentations, including random flips, rotations, and transpositions, are applied to the teacher’s input. Moving to a stronger augmentation level, the student receives intensive-based transformations in unsupervised phase, such as color jittering, auto-contrast and Gaussian noise with a random distortion strength, which enlarges the recognition space and prevents overfitting to the teacher’s predictions.

At the highest noise level, structured perturbations are injected into the the student’s noisy decoder. Specifically, we adopt F-noise from [32], where uniform noise $\mathcal{N} \sim \mathcal{U}(-0.3, 0.3)$ is sampled with the same size of the encoder’s output. The perturbed encoder’s feature representation is then computed as $\tilde{\mathbf{Z}}_s = (\mathbf{Z}_s \odot \mathcal{N}) + \mathbf{Z}_s$.

In supervised phase, the labeled input x^l is transformed into weak augmented versions, then the labels y^l guide both student’s decoders outputs:

$$p^1 = \mathcal{D}_s^1(\mathcal{E}_s(\mathcal{A}_w(x^l))), \quad p^2 = \mathcal{D}_s^2(\text{Noise}(\mathcal{E}_s(\mathcal{A}_w(x^l)))), \tag{6}$$

we eliminate the Softmax term applied on p^k for efficient, the supervised loss is then computed as:

$$\mathcal{L}_{\text{sup}} = \sum_{k=1}^2 \frac{1}{M} \sum_{i=1}^M \frac{1}{H \cdot W} \sum_{j=1}^{H \cdot W} \mathcal{L}_{\text{ce}}(p_{ij}^k, y_{ij}^l), \tag{7}$$

where M is the number of labeled images, \mathcal{L}_{ce} is the pixel-wise cross-entropy loss, p_{ij}^k is the student’s decoder prediction, and Noise represents noise injection applied to the noisy student’s decoder. The details of the unsupervised phase will be presented in the following sections.

3.3. Hierarchical Distillation for Multi-Level Noisy Consistency

In the unsupervised phase, the overall training objective consists of three primary loss functions: Correlation Guidance Loss, which aligns the teacher and student’s main decoder representations; Mutual Information Loss, which maximizes information sharing between the two student decoders; and Pixel-level Consistency Loss, which ensures consistency between the probability outputs of the teacher and student models (Figure 1).

3.3.1. Correlation Guidance Loss

To ensure that the student’s learned features are structurally aligned with the teacher’s representations, we employ a correlation guidance loss. This loss is inspired by the concept of cross-correlation in self-supervised learning [48], where

highly correlated representations indicate strong knowledge transfer.

Given a batch of normalized final feature representations from the student $\mathbf{Z}_s \in \mathbb{R}^{b \times d}$ and the teacher $\mathbf{Z}_t \in \mathbb{R}^{b \times d}$, where b is the batch size, we compute the cross-correlation matrix:

$$\mathcal{C}_{st} = \frac{\mathbf{Z}_s^T \mathbf{Z}_t}{b} \quad (8)$$

A perfect correlation between the student and teacher representations is achieved when the diagonal entries $(\mathcal{C}_{st})_{ii}$ are all equal to 1. To enforce this, we define the correlation loss as:

$$\mathcal{L}_{CG} = \log_2 \sum_{i=1}^d ((\mathcal{C}_{st})_{ii} - 1)^{2\alpha}, \quad (9)$$

where α is a hyperparameter that controls the penalty for deviations from perfect correlation. A larger α enforces stronger alignment between the student and the teacher representations. For computational efficiency, we set $\alpha = 2$.

3.3.2. Mutual Information Loss

To further enhance knowledge transfer, we move beyond feature-wise alignment and incorporate intra-batch consistency through a mutual information loss. While the correlation loss ensures that the student’s main decoder is well-aligned with the teacher, it does not explicitly enforce consistency between the student’s two decoders. To address this, we establish a hierarchical distillation scheme, where knowledge is not only transferred from the teacher to the main decoder but also propagated from the main decoder to the noisy one. This structured flow of information ensures that both decoders develop robust representations while simultaneously allowing the shared encoder to learn complementary features from both branches.

Given the Gram matrices of the student’s main decoder, K^1 and the noisy decoder, K^2 , we compute their Hadamard product:

$$K^{12} = K^1 \circ K^2, \quad (10)$$

which K^{12} is normalized to ensure unit trace to preserve scale invariance. The mutual information loss is then formulated as:

$$\mathcal{L}_{MI} = -I(K^1, K^2) = H_\alpha(K^{12}) - H_\alpha(K^2), \quad (11)$$

where H_α denotes the entropy term parameterized by α . Compared to Equation 3.1, the term K^1 is omitted since we stop the gradient of the main decoder’s output at this stage. Maximizing the mutual information encourages the student’s decoders to preserve the intra-batch relationships for transferring structured knowledge across perturbation levels.

3.3.3. Pixel-Level Consistency Loss

To enforce fine-grained alignment between the teacher’s predictions and the student’s decoders, we introduce a pixel-level consistency loss. Unlike the correlation and mutual

information losses, which focus on feature representations, this loss directly minimizes the discrepancy between the teacher’s predicted outputs and the outputs of both student decoders.

Let $\hat{y} = \mathcal{T}(\mathcal{A}_w(x^u))$ denote the teacher’s predicted probability map, while p_u^1 and p_u^2 represent the outputs of the student’s main and noisy decoders, respectively, given strongly augmented inputs $\mathcal{A}_s(x)$. To enforce consistency between the student’s predictions and the teacher’s guidance, we define the pixel-level consistency loss as:

$$\mathcal{L}_{pix} = \|p_u^1 - \hat{y}\|_2^2 + \|p_u^2 - \hat{y}\|_2^2 \quad (12)$$

This loss ensures that both decoders produce outputs that remain close to the teacher’s predictions, thereby enforcing stable predictions while preserving pixel-wise alignment.

3.4. Final Objective Function

The final loss function combines supervised loss together with knowledge distillation losses:

$$\mathcal{L}_{total} = \mathcal{L}_{sup} + \beta_{CG} \mathcal{L}_{CG} + \beta_{MI} \mathcal{L}_{MI} + \mathcal{L}_{pix}, \quad (13)$$

where β_{CG} and β_{MI} are weighting hyper-parameters regulate the interplay between correlation guidance from the teacher and the student’s mutual information preservation.

3.5. Progressive Parameter Updates

The teacher model is updated using an exponential moving average (EMA) of the student with main decoder:

$$\theta_t \leftarrow \alpha \theta_t + (1 - \alpha) \theta_s^1, \quad (14)$$

where α is the EMA smoothing factor, and θ_t and θ_s^1 denote the weights of the teacher and the student, respectively.

The student parameters are updated based on the total loss:

$$\theta_s \leftarrow \theta_s + \eta \frac{\partial(\mathcal{L}_{total})}{\partial \theta_s} \quad (15)$$

It is worth noting that the main decoder is excluded from updates by the mutual information loss to preserve its alignment with the teacher.

4. Experiments and Results

4.1. Dataset

The Fetal Ultrasound Grand Challenge (FUGC) dataset: Semi-Supervised Cervical Segmentation [1] from ISBI 2025 is employed, containing 500 transvaginal ultrasound images of the uterine cervix. This dataset includes 50 labeled images and 450 unlabeled ones. For training, 40 labeled images are used, while 10 are reserved for validation. The test set consists of 90 images sourced from the challenge’s Validation Phase [1].

Backbone	Method	40/450		20/470		10/480	
		DSC \uparrow	HD \downarrow	DSC \uparrow	HD \downarrow	DSC \uparrow	HD \downarrow
ResNet50	SupOnly	0.8360	50.91	0.8012	59.02	0.7732	66.03
	Mean Teacher (NeurIPS'17)	0.8602	49.12	0.8372	53.15	0.8177	60.20
	FixMatch (NeurIPS'20)	0.8666	38.82	0.8347	54.14	0.8192	59.81
	CPS (CVPR'21)	0.8590	43.12	0.8321	56.08	0.8130	61.00
	PS-MT (CVPR'22)	0.8621	47.00	0.8401	51.99	0.8213	59.37
	CCVC (CVPR'23)	0.8597	41.09	0.8325	55.78	0.8165	60.42
	Dual Teacher (NeurIPS'23)	0.8672	42.70	0.8413	51.38	0.8203	59.55
	AD-MT (ECCV'24)	0.8700	39.99	0.8427	50.66	0.8230	59.04
	HDC	0.8704	38.97	0.8503	48.73	0.8299	57.82
ResNet101	SupOnly	0.8542	39.17	0.8137	57.45	0.7798	63.89
	Mean Teacher (NeurIPS'17)	0.8862	47.40	0.8298	51.58	0.8201	59.59
	FixMatch (NeurIPS'20)	0.8874	33.36	0.8402	52.11	0.8221	59.21
	CPS (CVPR'21)	0.8739	38.20	0.8398	51.02	0.8169	60.58
	PS-MT (CVPR'22)	0.8870	40.34	0.8420	56.25	0.8234	58.97
	CCVC (CVPR'23)	0.8791	36.67	0.8409	48.86	0.8199	59.62
	Dual Teacher (NeurIPS'23)	0.8898	38.86	0.8498	48.63	0.8242	58.83
	AD-MT (ECCV'24)	0.8910	36.92	0.8507	46.78	0.8239	58.88
	HDC	0.8983	36.50	0.8580	45.51	0.8331	57.13

Table 1. Quantitative results on FUGC of different semi-supervised learning methods under three data ratios. The best result is in **bold**.

To further validate the model’s generalization capacity, experiments are conducted on the MICCAI 2023 Grand Challenge - PSFH dataset [21], specifically focusing on the segmentation of the pubic symphysis (PS) and fetal head (FH). The dataset consists of 5,101 photos divided into three subsets: training (70%), validation (10%), and testing (20%). Each image is linked with a precise segmentation mask that delineates the FH and PS, allowing for the successful construction and evaluation of relevant segmentation models.

4.2. Implementation Details

The experimental setup is based on PyTorch, utilizing an NVIDIA RTX 3090Ti with 24GB VRAM. All experiments were conducted on an Ubuntu 20.04 operating system with Python 3.8, PyTorch 1.10, and CUDA 11.3.

For the FUGC dataset, the AdamW optimizer is employed with an initial learning rate of 1×10^{-4} , $\beta_{CG} = 0.9$, $\beta_{MI} = 0.999$, $\epsilon = 1 \times 10^{-8}$, and a weight decay of 0.05. A CosineAnnealingLR scheduler is applied to ensure smooth convergence throughout training.

For the PSFH Dataset, we used the same setting as DSTCT [13]. Using the Stochastic Gradient Descent (SGD) optimizer set up with a momentum of 0.9 and a weight decay of 0.0001, the network training protocol involved

30,000 iterations. To accommodate semi-supervised learning paradigms, we used a batch size 16, with an equal distribution of eight tagged and eight unlabeled photos. A clustering-based learning rate technique was used to modify the training’s initial learning rate of 0.01 dynamically. Data noise perturbation in the $[-0.2, 0.2]$ range was added to improve the model’s resilience to input variability

4.3. Evaluation Metrics

Similar to the ISBI Challenge’s original assessment criteria, we validated the model’s performance by employing Hausdorff Distance (HD) and Dice Score for the FUGC dataset.

Three recognized metrics—the Average Surface Distance (ASD), the 95% Hausdorff Distance (HD95), and the Dice Similarity Coefficient (DSC)—were used to assess these models’ performance on the PSFH dataset statistically. Thanks to these parameters, the accuracy and consistency of the segmentation models can be thoroughly evaluated, which is essential for confirming their clinical usefulness.

4.4. Quantitative Results

In this experiment, we compare HDC with existing approaches to semi-supervised learning. Unlike previous methods, HDC consists of one student and one teacher,

Method	PS			FH			PSFH		
	DSC↑	ASD↓	HD ₉₅ ↓	DSC↑	ASD↓	HD ₉₅ ↓	DSC↑	ASD↓	HD ₉₅ ↓
SupOnly	0.835	0.793	3.875	0.897	1.901	8.868	0.866	1.347	6.372
MT [39]	0.803	0.760	5.143	0.872	2.912	13.608	0.837	1.836	9.376
ICT [43]	0.847	0.813	3.806	0.896	1.694	7.191	0.871	1.254	5.498
UAMT [47]	0.830	0.801	4.375	0.889	1.661	7.296	0.859	1.231	5.836
DAN [50]	0.824	1.048	4.583	0.866	1.443	8.871	0.855	1.246	5.727
DCT [34]	0.801	1.009	4.960	0.879	2.081	9.044	0.840	1.545	7.002
CCT [32]	0.824	0.596	4.388	0.886	2.693	11.604	0.855	1.645	7.998
CPS [5]	0.829	0.701	3.788	0.893	1.385	5.952	0.864	1.043	4.870
CTCT [22]	0.836	0.794	4.265	0.888	3.440	6.163	0.859	1.231	5.807
CTCL [18]	0.826	1.197	5.509	0.900	0.747	5.107	0.863	0.972	5.308
S4CVnet [45]	0.838	0.823	3.926	0.906	0.975	4.658	0.872	0.899	4.310
DSTCT [13]	0.845	0.602	4.013	0.912	0.496	3.982	0.879	0.549	3.998
HDC	0.850	0.605	3.911	0.928	0.466	3.434	0.889	0.536	3.673

Table 2. Quantitative results on PSFH of different semi-supervised learning methods under three data ratios. The best result is in **bold**.

where the student has two decoders to enhance both consistency learning and multi-task supervision.

Table 1 summarizes the segmentation performance of different methods under varying labeled/unlabeled data splits. HDC outperforms previous state-of-the-art methods across most settings. Specifically, under the ResNet50 backbone, our method achieves 0.8704 Dice and 38.97 HD in the 40/450 setting, slightly behind FixMatch [37], which achieves the best HD of 38.82. Similarly, under ResNet101, FixMatch also achieves the lowest HD of 33.36, indicating its strong ability to reduce boundary errors in the high-data regime.

However, when the number of labeled images decreases to 20 or 10, our method achieves the best performance across both ResNet50 and ResNet101 backbones. Specifically, under the 20/470 setting, our approach achieves the highest Dice scores of 0.8503 (ResNet50) and 0.8580 (ResNet101) while also obtaining the best HD scores of 48.73 (ResNet50) and 45.51 (ResNet101). Similarly, in the most challenging 10/480 setting, our method maintains the best Dice scores of 0.8299 (ResNet50) and 0.8331 (ResNet101) and the lowest HD scores of 57.82 and 57.13, respectively.

Table 2 presents the quantitative outcomes on the PSFH dataset when trained with only 20% of the total labeled training data, demonstrating the effectiveness of semi-supervised learning in leveraging unlabeled data for fetal ultrasound segmentation. Despite the significantly reduced annotation requirement, HDC consistently outperforms state-of-the-art approaches across all segmentation

tasks. Specifically, model achieves a DSC of 0.850 for the PS task, surpassing DSTCT (0.845) and significantly outperforming MT (0.803). In the FH task, HDC attains a DSC of 0.928 and an HD₉₅ of 3.434, improving upon DSTCT (0.920 DSC, 3.493 HD₉₅) and ICT (0.916 DSC, 7.191 HD₉₅). Similarly, for the PSFH task, our method achieves the highest DSC (0.889) and the lowest HD₉₅ (3.673), outperforming all other techniques. These results highlight the strong generalization capability of our hierarchical distillation strategy, which allows the model to learn from unlabeled data more effectively.

4.5. Qualitative Result

The qualitative results in Fig. 3 illustrate the segmentation performance of different methods on transvaginal ultrasound images. The supervised-only approach exhibits the weakest performance, with noticeable segmentation errors compared to the ground truth, which is expected due to its inability to leverage unlabeled data. AD-MT produces improved results, but noticeable deviations from the GT remain, particularly in boundary regions. In contrast, HDC achieves the closest segmentation to the GT, capturing finer details and reducing misclassified regions, demonstrating the effectiveness of our semi-supervised approach in leveraging unlabeled data for enhanced segmentation accuracy.

4.6. Ablation studies

To analyze the contribution of different loss components, we conduct an ablation study in Table 3. HDC integrates Pix Loss, CG Loss, and MI Loss, with the full combination

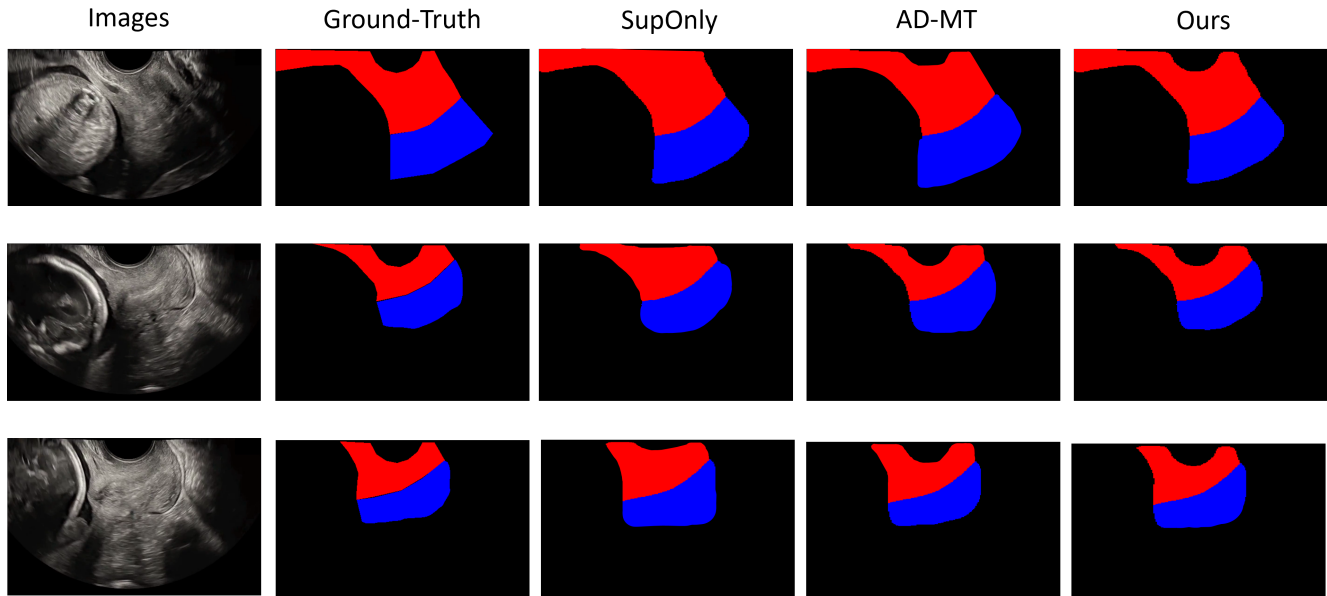


Figure 3. Qualitative comparison of different semi-supervised segmentation methods results.

Method			40/450	
Pix Loss	CG Loss	MI Loss	Dice	HD
✓			0.8889	38.55
✓	✓		0.8881	38.72
✓		✓	0.8904	38.03
✓	✓	✓	0.8983	36.50

Table 3. Ablation study of different loss components on the 40/450 setting.

yielding the highest Dice score of 0.8983 and the lowest HD of 36.50. These results indicate that each loss function contributes to better segmentation quality, and their synergy further enhances performance. HDC effectively leverages unlabeled data through consistency training, outperforming prior semi-supervised methods, particularly in low-label settings (20/470 and 10/480). The dual-decoder structure improves feature representation, leading to superior Dice scores and Hausdorff Distance reductions across most experimental settings.

5. Conclusion

This work presents a novel semi-supervised segmentation framework for transvaginal ultrasound imaging, addressing challenges like low contrast and shadow artifacts through adaptive consistency learning with a single-teacher architecture. By introducing Correlation Guidance Loss and Mutual Information Loss, the framework enhances fea-

ture alignment and stabilizes student learning while reducing computational complexity. Experimental results on FUGC and PSFH datasets demonstrate state-of-the-art performance with lower computational overhead than multi-teacher models, highlighting its effectiveness and generalization ability. This approach offers a promising direction for efficient medical image segmentation, with potential future applications across various imaging modalities.

Acknowledgement

We acknowledge the support from University of Information Technology (UIT), and AI VIETNAM Lab for providing the GPU for the numerical calculations.

References

- [1] Jieyun Bai, Ziduo Yang, Kamrul Hasan, Jie Gan, Zhuonan Liang, Weidong Cai, Tao Tan, Jing Ye, Mohammad Yaqub, Dong Ni, Saad Slimani, Benard Ohene-Botwe, Campello Manuel, and Karim Lekadir. Fetal ultrasound grand challenge: Semi-supervised cervical segmentation (fugc25), 2024. 1, 2, 5
- [2] Paola Cascante-Bonilla, Fuwen Tan, Yanjun Qi, and Vicente Ordonez. Curriculum labeling: Revisiting pseudo-labeling for semi-supervised learning. In *Proceedings of the AAAI conference on artificial intelligence*, pages 6912–6920, 2021. 2
- [3] Defang Chen, Jian-Ping Mei, Hailin Zhang, Can Wang, Yan Feng, and Chun Chen. Knowledge distillation with the reused teacher classifier. In *Proceedings of the IEEE/CVF conference on computer vision and pattern recognition*, pages 11933–11942, 2022. 3

- [4] Pengguang Chen, Shu Liu, Hengshuang Zhao, and Jiaya Jia. Distilling knowledge via knowledge review. In *Proceedings of the IEEE/CVF conference on computer vision and pattern recognition*, pages 5008–5017, 2021. 3
- [5] Xiaokang Chen, Yuhui Yuan, Gang Zeng, and Jingdong Wang. Semi-supervised semantic segmentation with cross pseudo supervision. In *IEEE Conference on Computer Vision and Pattern Recognition (CVPR)*, 2021. 2, 7
- [6] Thomas M Cover. *Elements of information theory*. John Wiley & Sons, 1999. 3
- [7] Jianping Gou, Baosheng Yu, Stephen J Maybank, and Dacheng Tao. Knowledge distillation: A survey. *International Journal of Computer Vision*, 129(6):1789–1819, 2021. 4
- [8] Yuxin Guo, Shijie Ma, Hu Su, Zhiqing Wang, Yuhao Zhao, Wei Zou, Siyang Sun, and Yun Zheng. Dual mean-teacher: An unbiased semi-supervised framework for audio-visual source localization. *Advances in Neural Information Processing Systems*, 36:48639–48661, 2023. 2
- [9] Ziyao Guo, Haonan Yan, Hui Li, and Xiaodong Lin. Class attention transfer based knowledge distillation. In *Proceedings of the IEEE/CVF Conference on Computer Vision and Pattern Recognition*, pages 11868–11877, 2023. 3
- [10] Geoffrey Hinton, Oriol Vinyals, and Jeff Dean. Distilling the knowledge in a neural network. *arXiv preprint arXiv:1503.02531*, 2015. 3
- [11] Seunghoon Hong, Hyeonwoo Noh, and Bohyung Han. Decoupled deep neural network for semi-supervised semantic segmentation. *Advances in neural information processing systems*, 28, 2015. 2
- [12] Tao Huang, Shan You, Fei Wang, Chen Qian, and Chang Xu. Knowledge distillation from a stronger teacher. *Advances in Neural Information Processing Systems*, 35:33716–33727, 2022. 3
- [13] Jianmei Jiang, Huijin Wang, Jieyun Bai, Shun Long, Shuangping Chen, Victor M Campello, and Karim Lekadir. Intrapartum ultrasound image segmentation of pubic symphysis and fetal head using dual student-teacher framework with cnn-vit collaborative learning. In *International conference on medical image computing and computer-assisted intervention*, pages 448–458. Springer, 2024. 6, 7
- [14] Ying Jin, Jiaqi Wang, and Dahua Lin. Multi-level logit distillation. In *Proceedings of the IEEE/CVF Conference on Computer Vision and Pattern Recognition*, pages 24276–24285, 2023. 3
- [15] Minh-Dung Le-Quynh, Anh-Tuan Nguyen, Anh-Tuan Quang-Hoang, Van-Huy Dinh, Tien-Huy Nguyen, Hoang-Bach Ngo, and Minh-Hung An. Enhancing video retrieval with robust clip-based multimodal system. In *Proceedings of the 12th International Symposium on Information and Communication Technology*, pages 972–979, 2023. 3
- [16] Semi-Supervised Learning. Semi-supervised learning. *CS22006.html*, 5(2):1, 2006. 2
- [17] Dong-Hyun Lee et al. Pseudo-label: The simple and efficient semi-supervised learning method for deep neural networks. In *Workshop on challenges in representation learning, ICML*, page 896. Atlanta, 2013. 2
- [18] Wei Li and Huihua Yang. Collaborative transformer-cnn learning for semi-supervised medical image segmentation. In *2022 IEEE International Conference on Bioinformatics and Biomedicine (BIBM)*, pages 1058–1065. IEEE, 2022. 7
- [19] Chen Liang, Wenguan Wang, Jiayu Miao, and Yi Yang. Logic-induced diagnostic reasoning for semi-supervised semantic segmentation. In *Proceedings of the IEEE/CVF International Conference on Computer Vision*, pages 16197–16208, 2023. 2
- [20] Yuyuan Liu, Yu Tian, Yuanhong Chen, Fengbei Liu, Vasileios Belagiannis, and Gustavo Carneiro. Perturbed and strict mean teachers for semi-supervised semantic segmentation. In *Proceedings of the IEEE/CVF conference on computer vision and pattern recognition*, pages 4258–4267, 2022. 2
- [21] Yaosheng Lu, Mengqiang Zhou, Dengjiang Zhi, Minghong Zhou, Xiaosong Jiang, Ruiyu Qiu, Zhanhong Ou, Huijin Wang, Di Qiu, Mei Zhong, et al. The jnu-ifm dataset for segmenting pubic symphysis-fetal head. *Data in brief*, 41: 107904, 2022. 2, 6
- [22] Xiangde Luo, Minhao Hu, Tao Song, Guotai Wang, and Shaoting Zhang. Semi-supervised medical image segmentation via cross teaching between cnn and transformer. In *International conference on medical imaging with deep learning*, pages 820–833. PMLR, 2022. 7
- [23] Quoc-Vinh Luu, Khanh-Duy Le, Thanh-Huy Nguyen, Thanh-Minh Nguyen, Quan Nguyen, Tien-Thinh Nguyen, and Quang-Vinh Dinh. Semi-supervised semantic segmentation using redesigned self-training for white blood cells. In *2025 IEEE 6th International Conference on Image Processing, Applications and Systems (IPAS)*, pages 1–6. IEEE, 2025. 2
- [24] Kangfu Mei, Mauricio Delbracio, Hossein Talebi, Zhengzhong Tu, Vishal M Patel, and Peyman Milanfar. Conditional diffusion distillation. 2023. 3
- [25] Roy Miles, Ismail Elezi, and Jiankang Deng. Vkd: Improving knowledge distillation using orthogonal projections. In *Proceedings of the IEEE/CVF Conference on Computer Vision and Pattern Recognition*, pages 15720–15730, 2024. 3
- [26] Jaemin Na, Jung-Woo Ha, Hyung Jin Chang, Dongyoon Han, and Wonjun Hwang. Switching temporary teachers for semi-supervised semantic segmentation. *Advances in Neural Information Processing Systems*, 36:40367–40380, 2023. 2
- [27] Ba Hung Ngo, Ba Thinh Lam, Thanh Huy Nguyen, Quang Vinh Dinh, and Tae Jong Choi. Dual dynamic consistency regularization for semi-supervised domain adaptation. *IEEE Access*, 2024. 2
- [28] Huy Thanh Nguyen, Thinh Ba Lam, Toan Thai Ngoc Truong, Thang Dinh Duong, and Vinh Quang Dinh. Mv-trams: An efficient tumor region-adapted mammography synthesis under multi-view diagnosis. *Available at SSRN 5109180*. 2
- [29] Thanh-Huy Nguyen, Thi Kim Ngan Ngo, Mai Anh Vu, and Ting-Yuan Tu. Blurry-consistency segmentation framework with selective stacking on differential interference contrast 3d breast cancer spheroid. In *Proceedings of the IEEE/CVF Conference on Computer Vision and Pattern Recognition*, pages 5223–5230, 2024. 2

- [30] Tien-Huy Nguyen, Quang-Khai Tran, and Anh-Tuan Quang-Hoang. Improving generalization in visual reasoning via self-ensemble. *arXiv preprint arXiv:2410.20883*, 2024. 3
- [31] Tho-Quang Nguyen, Huu-Loc Tran, Tuan-Khoa Tran, Huu-Phong Phan-Nguyen, and Tien-Huy Nguyen. Fa-yolov9: Improved yolov9 based on feature attention block. In *2024 International Conference on Multimedia Analysis and Pattern Recognition (MAPR)*, pages 1–6. IEEE, 2024. 2
- [32] Yassine Ouali, Celine Hudelot, and Myriam Tami. Semi-supervised semantic segmentation with cross-consistency training. In *The IEEE/CVF Conference on Computer Vision and Pattern Recognition (CVPR)*, 2020. 2, 4, 7
- [33] Vuong Pham et al. Robust engineering-based unified biomedical imaging framework for liver tumor segmentation. *Current Medical Imaging Reviews*, 19(1):37–45, 2023. 2
- [34] Siyuan Qiao, Wei Shen, Zhishuai Zhang, Bo Wang, and Alan Yuille. Deep co-training for semi-supervised image recognition. In *Proceedings of the european conference on computer vision (eccv)*, pages 135–152, 2018. 7
- [35] Alfréd Rényi. On measures of entropy and information. In *Proceedings of the fourth Berkeley symposium on mathematical statistics and probability, volume 1: contributions to the theory of statistics*, pages 547–562. University of California Press, 1961. 3
- [36] Mamshad Nayeem Rizve, Kevin Duarte, Yogesh S Rawat, and Mubarak Shah. In defense of pseudo-labeling: An uncertainty-aware pseudo-label selection framework for semi-supervised learning. *arXiv preprint arXiv:2101.06329*, 2021. 2
- [37] Kihyuk Sohn, David Berthelot, Nicholas Carlini, Zizhao Zhang, Han Zhang, Colin A Raffel, Ekin Dogus Cubuk, Alexey Kurakin, and Chun-Liang Li. Fixmatch: Simplifying semi-supervised learning with consistency and confidence. *Advances in neural information processing systems*, 33:596–608, 2020. 2, 7
- [38] Suraj Srinivas and François Fleuret. Knowledge transfer with jacobian matching. In *International Conference on Machine Learning*, pages 4723–4731. PMLR, 2018. 3
- [39] Antti Tarvainen and Harri Valpola. Mean teachers are better role models: Weight-averaged consistency targets improve semi-supervised deep learning results. *Advances in neural information processing systems*, 30, 2017. 2, 7
- [40] Nguyen ND Tran et al. Segmentation on chest ct imaging in covid-19 based on the improvement attention u-net model. In *New trends in intelligent software methodologies, tools and techniques*, pages 596–606. IOS Press, 2022. 1
- [41] Thi-Oanh Tran, Thanh-Huy Nguyen, Tuan Tung Nguyen, and Nguyen Quoc Khanh Le. Mlg2net: Molecular global graph network for drug response prediction in lung cancer cell lines. *Journal of Medical Systems*, 49(1):1–7, 2025. 3
- [42] Tim Van Erven and Peter Harremo. Rényi divergence and kullback-leibler divergence. *IEEE Transactions on Information Theory*, 60(7):3797–3820, 2014. 3
- [43] Vikas Verma, Kenji Kawaguchi, Alex Lamb, Juho Kannala, Arno Solin, Yoshua Bengio, and David Lopez-Paz. Interpolation consistency training for semi-supervised learning. *Neural Networks*, 145:90–106, 2022. 7
- [44] Karel Veselý, Mirko Hannemann, and Lukáš Burget. Semi-supervised training of deep neural networks. In *2013 IEEE Workshop on Automatic Speech Recognition and Understanding*, pages 267–272. IEEE, 2013. 2
- [45] Ziyang Wang, Tianze Li, Jian-Qing Zheng, and Baoru Huang. When cnn meet with vit: Towards semi-supervised learning for multi-class medical image semantic segmentation. In *European conference on computer vision*, pages 424–441. Springer, 2022. 7
- [46] Zicheng Wang, Zhen Zhao, Xiaoxia Xing, Dong Xu, Xiangyu Kong, and Luping Zhou. Conflict-based cross-view consistency for semi-supervised semantic segmentation. In *Proceedings of the IEEE/CVF conference on computer vision and pattern recognition*, pages 19585–19595, 2023. 2
- [47] Lequan Yu, Shujun Wang, Xiaomeng Li, Chi-Wing Fu, and Pheng-Ann Heng. Uncertainty-aware self-ensembling model for semi-supervised 3d left atrium segmentation. In *Medical image computing and computer assisted intervention—MICCAI 2019: 22nd international conference, Shenzhen, China, October 13–17, 2019, proceedings, part II 22*, pages 605–613. Springer, 2019. 7
- [48] Jure Zbontar, Li Jing, Ishan Misra, Yann LeCun, and Stéphane Deny. Barlow twins: Self-supervised learning via redundancy reduction. In *International conference on machine learning*, pages 12310–12320. PMLR, 2021. 4
- [49] Bowen Zhang, Yidong Wang, Wenxin Hou, Hao Wu, Jindong Wang, Manabu Okumura, and Takahiro Shinozaki. Flexmatch: Boosting semi-supervised learning with curriculum pseudo labeling. *Advances in neural information processing systems*, 34:18408–18419, 2021. 2
- [50] Yizhe Zhang, Lin Yang, Jianxu Chen, Maridel Frederickson, David P Hughes, and Danny Z Chen. Deep adversarial networks for biomedical image segmentation utilizing unannotated images. In *Medical Image Computing and Computer Assisted Intervention—MICCAI 2017: 20th International Conference, Quebec City, QC, Canada, September 11–13, 2017, Proceedings, Part III 20*, pages 408–416. Springer, 2017. 7
- [51] Zhen Zhao, Zicheng Wang, Longyue Wang, Dian Yu, Yixuan Yuan, and Luping Zhou. Alternate diverse teaching for semi-supervised medical image segmentation. In *European Conference on Computer Vision*, pages 227–243. Springer, 2024. 2